Multifrequency Decoding of a Phased Array Doppler Sodar

I. SRINIVASA RAO, V. K. ANANDAN, AND M. SHRAVAN KUMAR

National Atmospheric Research Laboratory, Gadanki, India

ABSTRACT

Doppler sodar is being used for studying the lower part of atmospheric boundary layer (ABL) and wind profiling. To obtain maximum altitude coverage multifrequency transmission has been used along with more transmitted power. In this article, the implementation of multifrequency transmission of a Doppler sodar and its decoding to extract the atmospheric parameters are presented. This article also shows the advantage of profiling using multifrequency sodar operation. The range of frequency used for transmission is between 1700 and 2100 Hz. The decoded Doppler spectra have shown significant improvement in signal-to-noise ratio (SNR) as well as higher altitude coverage compared to single-frequency transmission and reception. Wind profiles obtained from sodar have been compared with data obtained from high-resolution GPS sonde balloons, which were launched from a place close to the sodar system. The authors observed that 30% more wind data height coverage in when transmission is in multifrequency mode; the consistency in wind estimate is also improved compared to the single-frequency transmission.

1. Introduction

Over the past three decades, the use of acoustic sounding (sodar) technique has led to significant advances in the studies of the atmospheric boundary layer. In its first implementation (McAllister 1968), the information provided is the intensity of the echoes as a function of height and time. Subsequent developments of the technique have been mainly directed to obtain vertical profiles of the radial wind component (Beran et al. 1971). During the last two decades, the scope of sodar applications has been enlarged considerably and covers a wide range of different fields, including convective boundary layer (CBL), formation of the nocturnal boundary layer (NBL), inversion layers, wind climatology below ABL, sound absorption in atmosphere, air pollution meteorology and weather forecasting, study of mesoscale flows and turbulence structure under stable and unstable stratification, and new technology development (Brown and Hall 1978; Mastrantonio and Fiocco 1982; Neff and Coulter 1986; Clifford et al. 1994; Giannini et al. 1996; Kramar and Kouznetsov 2002; Kallistratova and Coulter 2004; Coulter and Kallistratova 2004 and references therein; Kouznetsov et al. 2004, 2007; Engelbart et al. 2007).

Doppler sodar systems work by transmitting acoustic pulses upward into the atmosphere and by detecting the Doppler shift in the backscattered signal. Sodar sends and receives successive pulses of sound in different directions with different off-zenith angles. By measuring the intensity and frequency (Doppler shift) of the returned signal as a function of time, the radial velocity and thermal structure of the atmosphere can be determined. At least three beams in noncoplanar directions are needed in order to obtain zonal, meridional, and vertical wind velocity.

Sound energy propagates in the atmosphere as a longitudinal pressure wave and is attenuated as altitude increases. The attenuation of the sound wave as it propagates is frequency dependent, with higher frequency sound much more attenuated than lower frequency sound. With increasing temperatures or lower relative humidity, the attenuation of sound increases. Maximum range is typically achieved at locations that have low ambient noise and moderate-to-high relative humidity. In a dry atmosphere, sodar systems tend to have reduced altitude performance because of faster attenuation of acoustic waves. The background noise

Corresponding author address: V. K. Anandan, Radar Development Area, ISTRAC, Indian Space Research Organisation (ISRO), A 1-6, Peenya Industrial Estate, 1st Cross, Bangalore 560058, India.
E-mail: anandanvk@hotmail.com

where a sodar is operating can also limit its performance. The background acoustic energy spectrum (atmospheric acoustic noise) is heavily weighted toward the lower frequencies.

The pulse transmissions may include either single- or multifrequency sequences. It is, in principle, possible to operate the sodar at more than one acoustic frequency. Multifrequency sodar used to give better overall performance by using short-duration pulses at high frequencies and long-duration pulses at lower frequencies. The high frequencies are ideal to capture near-surface detail, but are attenuated very rapidly. Long wavelengths travel farther, but require longer pulses and range gates to ensure that their frequency characteristics are well defined for spectral analysis.

Sound waves travel with very low velocity when compared with electromagnetic waves, and it takes about 9 s to reach an altitude of 1.5 km. Hence, some of the signal processing techniques, such as coherent integration (time domain averaging) to improve the signal quality, are not possible to implement and that limits the performance of single-frequency transmission of sodar systems. Multifrequency transmission with frequency coding also can be used to get higher altitude coverage. This is possible by sending a sequence of pulses that have the same duration with different frequencies with same interpulse period.

There are sodar systems (Scintec–MFAS series) that are available commercially with multiple frequency transmission with range of frequencies (generally 1500–5000 Hz). Since these systems are patented, decoding and signal processing techniques being used are not available in the literature. This article presents the frequency decoding technique implemented for sodar at National Atmospheric Research Laboratory (NARL) and demonstrates its capability compared to single frequency transmission and reception.

2. System description

NARL phased array Doppler sodar system consists of 8×8 array of antenna elements made with piezoelectric transducers. Three elements from each corner have been removed to get the circular array pattern with a maximum sidelobe suppression of 17 dB. The transmission and reception are in reflected mode so the antenna with 52 elements is placed at a 70° inclination and the reflector at 35° with respect to the ground plane. This orientation makes the transmit/receive beam vertical to the horizontal plane when no beam tilting is applied. The NARL sodar can be operated with a frequency range of 1600 to 2500 Hz and is capable of transmitting multiple frequencies. A maximum of 10 different frequencies can be transmitted continuously. The piezoelectric tweeters generate 100-W acoustic power. The receiver is designed with a dynamic range of 70 dB. The pulse width and interpulse period is programmed to obtain a range resolution of 10 to 200 m for an altitude coverage of 1500 m. Observations can be conducted in three directions (east, north, vertical) with a tilt angle up to 22°. Detailed system description, signal processing techniques, and its performance may be obtained from Anandan et al. (2008).

Normally NARL sodar operates in single-frequency mode with a frequency of 1800 Hz. For this study, sodar is operated in single- and multifrequency modes with specifications shown in Table 1. Transmission starts with single-frequency mode with a frequency of 1800 Hz, after reception multifrequency transmission begins with five different frequencies from 1700 to 2100 Hz with a step of 100 Hz. This way, transmission continues in three directions (zenith, north, and east). The selected pulse width for transmission is 180 ms, which corresponds to a range resolution of 30 m. The experiment was conducted in a campaign mode for 20 days during November–December 2007 in clear-air conditions. During this period high-resolution GPS sonde balloons also launched from NARL close to the sodar site (less than 100 m). For validation of the multifrequency operation, the wind profiles obtained from the sodar observations were compared with winds obtained from the high-resolution GPS sonde balloons.

3. Analysis of multifrequency signals

In this section we present the method of retrieval of data from multifrequency signals. This method involves a sequence of steps applied on the time series data to obtain the single Doppler spectrum from multifrequency signals. For this analysis, five frequencies were considered for transmission from 1700 to 2100 Hz with a step of 100 Hz.

In multifrequency transmission the transmit pulse is comprised of five different frequencies: f_{t1}, f_{t2}, f_{t3}, f_{t4}, and f_{t5} with a separation of "f_{dif}" between successive frequencies. These frequencies were sent serially one after the other. All transmitted frequencies have same pulse width chosen at the time of experiment setup. The transmit sequence starts from lowest frequency f_{t1} (1700 Hz) and ends with highest frequency f_{t5} (2100 Hz). The Doppler-shifted backscattered echoes from the atmosphere received at the receiver in each range gate are f_{r1}, f_{r2}, f_{r3}, f_{r4}, and f_{r5}. Here, f_{r1} is the backscattered echo corresponding to the first transmitted frequency f_{t1}, f_{r2} belongs to the second transmitted frequency f_{t2}, and so on. Therefore, received echoes comprised of

Parameter	Value
Operating frequency	1.7–2.1 kHz
Pulse width	180 ms
Number of frequencies transmitted	5
Frequency increment	100 Hz
Beamwidth	5°
Acoustic power	100 W
Receiver gain	100 dB
Number of range gates	50
Range resolution	30 m
Number of FFT points	4098
Beam selection	Zenith, north 16°, east 16°

transmitted frequencies with Doppler shift (δf) corresponding to the transmitted frequencies

$$f_{r1} = f_{t1} \pm \delta f_1.$$

a. Step 1

The first step involved in this process is to convert the digitized backscattered time series signal into its equivalent power spectrum. This is done by applying fast Fourier transform on all the data points in each range gate so that power spectrum can be obtained for the entire range gates. A sample power spectrum observed in this analysis is shown in Fig. 1a. It consists of all the frequencies from 5 to 11 kHz, and this upper limit is determined by the sampling rate being used. But for better clarity, Fig. 1a is limited to the range of frequencies transmitted. From Fig. 1a one can see that there are five strong echoes related to transmitted frequencies. Because all the frequencies are transmitted sequentially and reception starts only after transmission of all frequencies, the multiple echoes at same range gate represent returns from different altitudes. That is, the echo f_{r1} corresponds to fifth range gate, f_{r2} corresponds to fourth range gate, f_{r3} corresponds to third range gate, f_{r4} corresponds to second range gate, and f_{r5} corresponds to first range gate. Because of this, in multifrequency transmission, the backscattered echoes f_{r1}, f_{r2}, f_{r3}, and f_{r4} correspond to the fourth, third, second, and first range gates, which are not present in the first few range gates. Therefore we lose the first four range gates data for f_{r1}, the first three range gates data for f_{r2}, the first two range gates data for f_{r3}, the first range gate data for f_{r4}, and f_{r5} is the only received signal having all range gates information. This is shown in Fig. 2. Time series data from different altitudes are stored for the complete observation window for further processing.

b. Step 2

Segment the data with a band of ±80 Hz with respect to each transmitted frequency and store each segment in a separate buffer for further processing. With this bandwidth, we can measure radial velocities maximum up to 6.08 m s^{-1} and horizontal velocities up to 22.1 m s^{-1} for all transmitted frequencies. This is because we can measure radial velocities maximum up to 7.76 m s^{-1} for first transmitted frequency f_{t1} and up to 6.08 m s^{-1} for last transmitted frequency f_{t5}. Here the first segment belongs to data of f_{t1}; that is, the 1700-Hz transmission, the second segment belongs to the 1800-Hz transmission, and so on. As explained in step 1, the last transmitted frequency will have data points from all the range gates, whereas for the other frequencies, it is one range gate less and it goes on increasing till reaches f_{t1}. Therefore we have now five segments corresponding to the five transmitted frequencies. Each segment consists of 50 range gates with altitude coverage of 1500 m. Unrepresented range gates of each frequency segments are filled with zeros.

c. Step 3

To identify the Doppler shift, the central or transmitted frequency is to be subtracted from the received frequency; that is,

$$\delta f_1 = f_{r1} - f_{t1}.$$

For the first segment, 1700 Hz is subtracted from 1700 $\pm\delta f_1$ for all range gates. Similarly for the remaining four segments, corresponding transmitted frequencies are subtracted. Now we have Doppler shift in terms of frequency (Hz). It is important to note that Doppler shifts obtained in all segments corresponding to one particular range gate are not same, since these are the backscattered echoes of five different frequencies. We know that, as frequency changes, wavelength changes and therefore velocity resolution will differ from one frequency to the other. The velocity resolution for the first transmitted frequency is 0.44 m s^{-1} and the last transmitted frequency is 0.55 m s^{-1}. Thus a Doppler shift of 1 Hz in the first segment corresponds to a radial velocity of 0.44 m s^{-1}, and the same Doppler shift of 1 Hz in the last segment corresponds to a radial velocity of 0.55 m s^{-1}. At this point, integrating the data of all segments will make no sense. Therefore to integrate the data in all segments, Doppler frequencies are to be converted into their equivalent radial velocities by multiplying it by half of its transmitted wavelength.
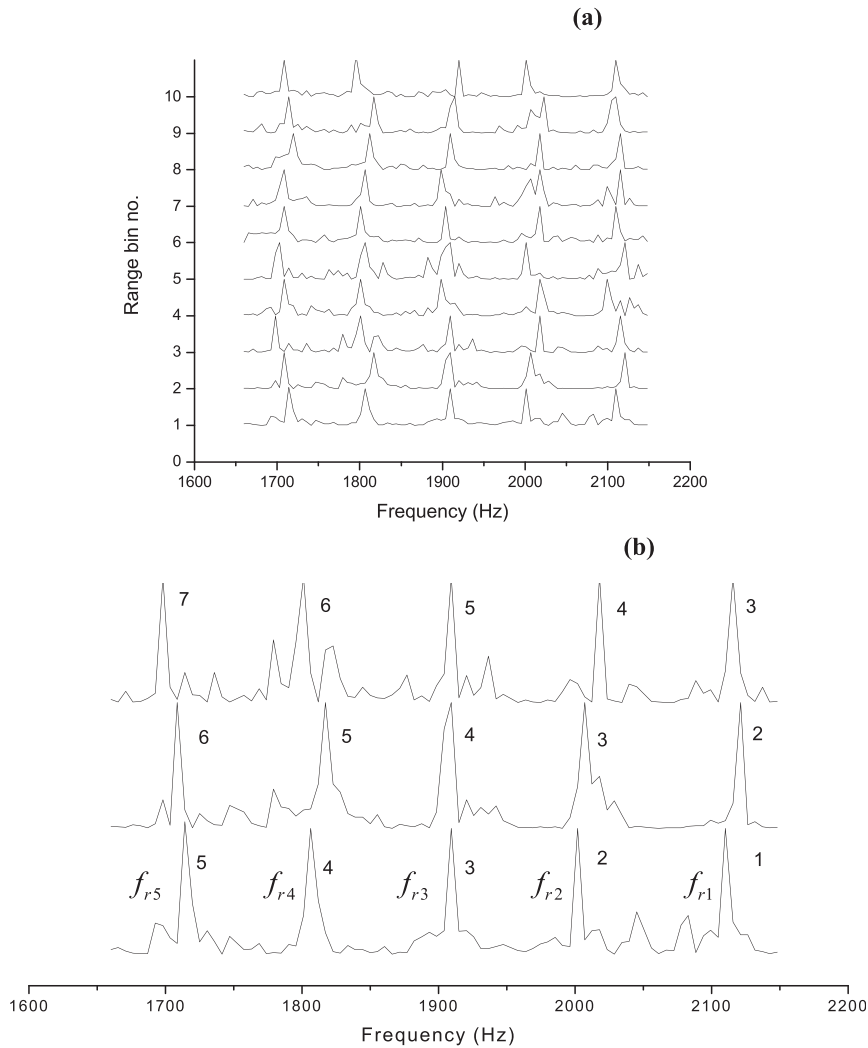
(a)

(b)

FIG. 1. (a) Sample power spectrum of multifrequency transmitted signal with five different frequencies. (b) Power spectrum of multifrequency output with five frequencies corresponding to different range gates, where numbers on the plot represent the range gate values.

d. Step 4

After converting Doppler frequencies into their equivalent radial velocities, an important step in this analysis is the spectral averaging; that is, integrating all the data segments corresponding to each range gate (incoherent integration)

$$P_i = \frac{1}{m} \sum_{k=1}^{m} P_{i,k} \quad i = 0, 1, 2, \ldots, N-1,$$

where P is the power spectral value, m is number of spectra integrated, and N is number of data points in each spectrum. The advantage of spectral averaging is that it improves the detectability of the Doppler spectrum. Incoherent integration increases the signal detrum. Incoherent integration increases the signal de-

tectability by a factor of $\sqrt{m}$ by reducing the noise variation (Farley 1985). The sample power spectrum after spectral averaging is shown in Fig. 2b. This completes the frequency decoding of the received backscattered echoes.

e. Step 5

The last step in this process is the estimation of lower order three moments, which represents power, mean Doppler velocity, and Doppler velocity width. Before extracting the moments, noise level is computed using the method followed by Hilderband and Sekhon (1974) and subtracted from each power spectral points. An adaptive moments estimation algorithm developed by Anandan et al. (2005) is used for the extraction of three moments with the expressions given by Woodman (1985).
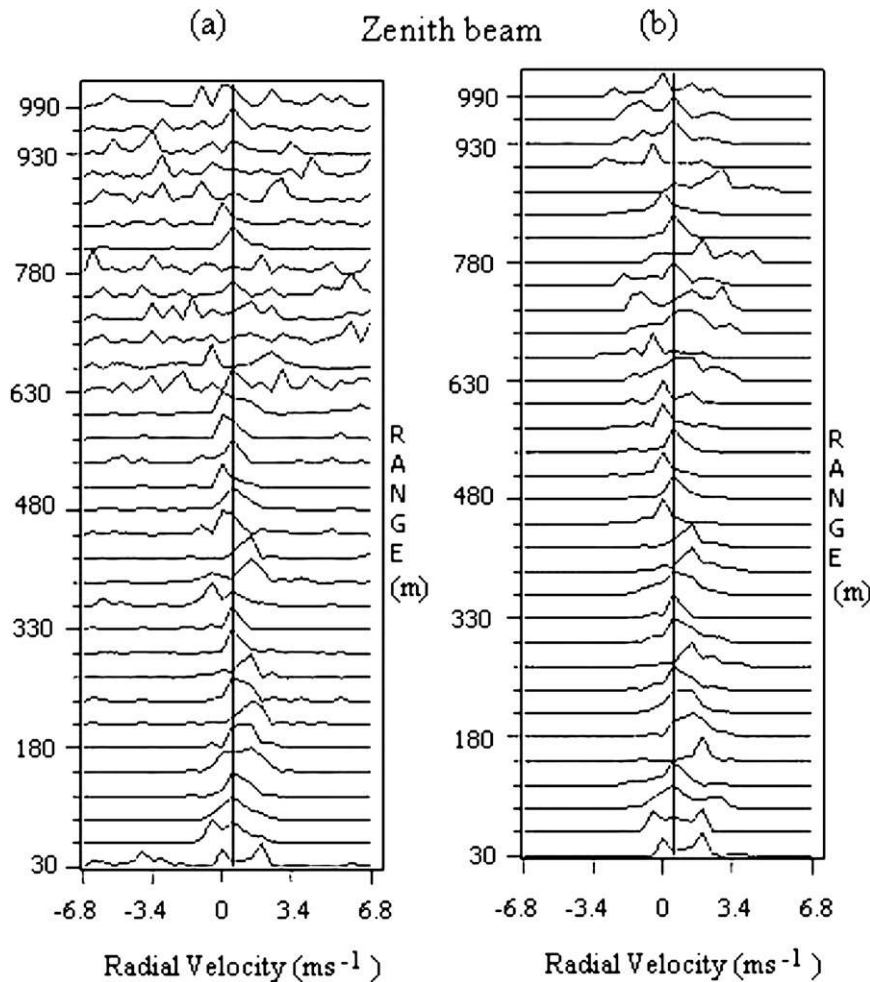
FIG. 2. Power spectrum plot derived from multifrequency coded signal for (a) single-frequency output and (b) multifrequency output for zenith beam.

Radial velocity is computed for three different directions (north 16°, east 16°, and zenith) to derive the horizontal wind velocity.

4. Results and discussion

As described above, after extracting the Doppler information, the three-dimensional zonal, meridional, and vertical wind velocities were derived for both single-frequency and multifrequency outputs. For validation of the data as well as the technique, the results have been compared with the simultaneous observations of high-resolution GPS sonde balloons. Figures 2a and 3a represents power spectrum of single-frequency (1800 Hz) transmission and Figs. 2b and 3b represent power spectrum of multifrequency transmission in the zenith, north, and east directions, respectively. From the figures it is observed that signal is well defined in multifre-

quency output in all beam directions and also that the height coverage is increased compared to single-frequency transmission and reception. Similar kinds of plots were obtained in the north. Most of our analysis consistently shows that 30% more height coverage is observed in multifrequency output than with single-frequency output. It is also observed that the power spectrum of multifrequency output has less noise when compared with single-frequency output and also backscattered echoes are easily traced in multifrequency output. This is caused by the reduction in noise variance in the velocity spectral averaging. Even though spectral averaging increases detectability, there is one more reason that might contribute to the height coverage. Generally backscattered signal is heavily weighted toward the scale size of the atmospheric targets, which varies in space and time. The scale size that matches the transmitted wavelength will contribute more to the backscattered signal. Even though
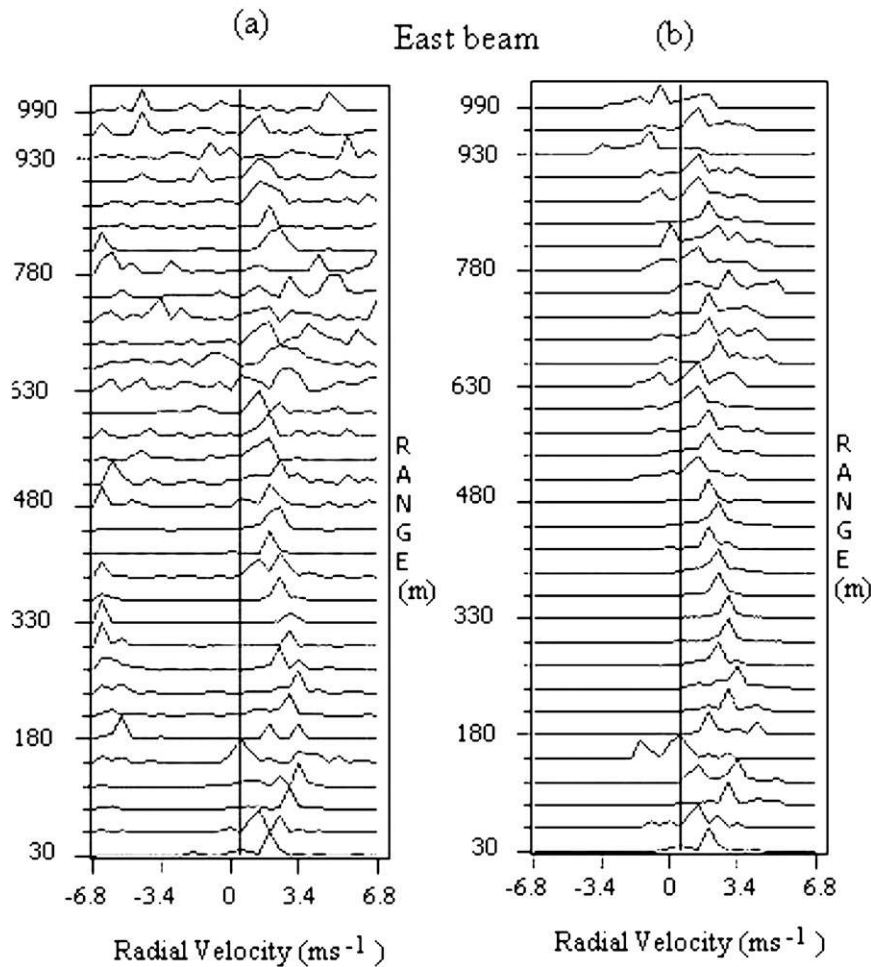
FIG. 3. Power spectrum plot derived from multifrequency coded signal for (a) single-frequency transmission and (b) multifrequency transmission for east beam.

atmospheric attenuation increases with increasing frequency, it is observed that signal strength is more for higher frequency transmission at some higher altitudes compared to low-frequency transmission. So in the case of multifrequency transmission, varied intensities are observed for the returned signal from the same range gate.

Figure 4 shows sample profile of horizontal wind measured by sodar and GPS sonde balloons on 21 November 2007. Similarly we have made wind profiles for twenty days of observations and presented them in terms of statistical parameters, such as standard deviation and correlation coefficient. Figure 4a corresponds to zonal velocity and Fig. 4b corresponds to meridional velocity obtained from single-frequency and multifrequency transmission along with GPS sonde balloon observations, which are considered by default to be standard reference. It is observed from the figure that the wind profile of single-frequency transmission com-

pares well with sonde profile up to 630 m, whereas in the case of multifrequency transmission, the profiles were in good match up to 960 m. Because of this, the statistics presented here are limited to 600 m for single-frequency transmission and up to 900 m for multifrequency transmission. Correlation analysis of horizontal winds derived from GPS sonde balloons and single-frequency sodar measurements during the campaign period is shown as a scatterplot in Fig. 5. There are 400 points plotted, and the correlation coefficient of 0.78 for zonal and 0.77 for meridional velocities is obtained. In general, small differences are expected between sodar and GPS sonde wind measurements because of temporal and spatial separation between two instruments and inherent biases and inaccuracies in the respective observational systems. So it is very important to note that any systematic bias introduced by the two systems and the general differences due to spatial separation will have similar affect on single-frequency and multifrequency transmission and
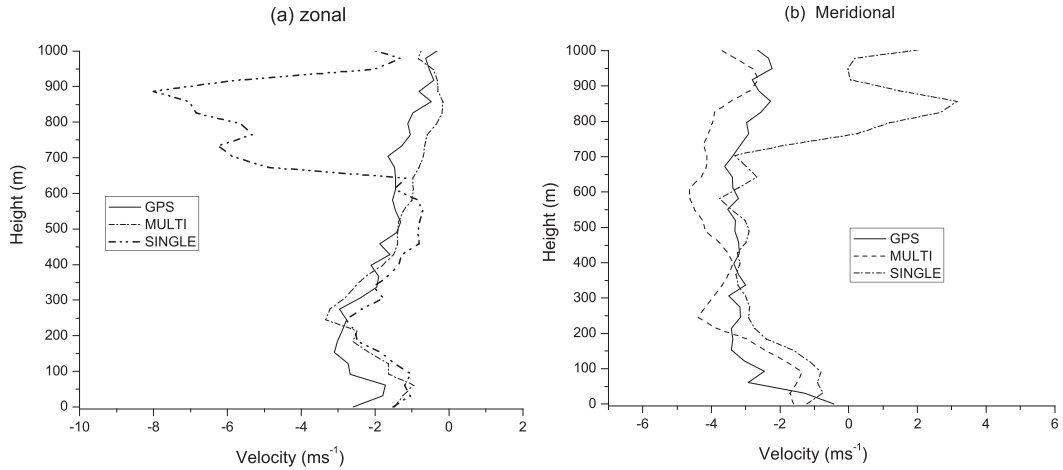
FIG. 4. Vertical profiles of (a) zonal and (b) meridional wind components measured by GPS sonde and sodar for single-frequency and multifrequency transmissions.

reception of the sodar system. It is also expected that in the multifrequency transmission and reception when the beam is tilted, different volumes of atmosphere are observed. If the frequency range being used is large (say 1500–5000 Hz), the beam can appear as much as 10° away from tilt angle for the furthest frequency of transmission (Kouznetsov 2008). In this case, the transmission frequency is in the range of 1700 to 2100 Hz, and the expected deviation from beam tilt angle is about ±1.5°. The 8 × 8 array has a beamwidth of 10.28° one way and 7.27° in two ways, so an additional tilt of 1.5° at the minimum and maximum frequency of transmission from the center frequency (say 1900 Hz) essentially looks like the same volume of information (within the beamwidth). Our results also show the signal returns are well comparable in all frequency in comparison with GPS sonde obser-

vation of wind velocity. One of the reasons for small discrepancy may be attributed to the small observation volume change in different frequency of transmission.

Scatterplots of sodar wind velocity derived in multifrequency transmission mode with GPS sonde wind velocity are shown in Fig. 6. Here, data is plotted up to a height of 900 m, corresponding to a total number of 600 points. The multifrequency sodar output has better correlation than single-frequency sodar output when compared with GPS sonde winds. The correlation coefficient found to be 0.82 for zonal and 0.80 for meridional velocity. Tables 2a and 2b show height statistics of correlation coefficient values for both single-frequency and multifrequency transmission. From the tables it is clear that in single-frequency transmission mode, sodar data is well-correlated with GPS sonde data up to a
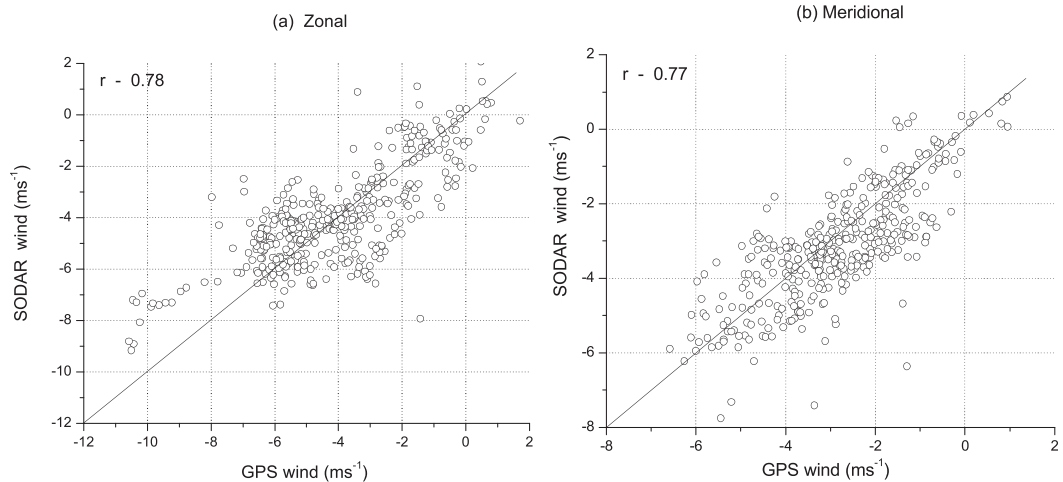

FIG. 5. Scatterplots of sodar wind velocity vs GPS sonde wind velocity for (a) zonal and (b) meridional components up to a height of 600 m in single-frequency output mode.
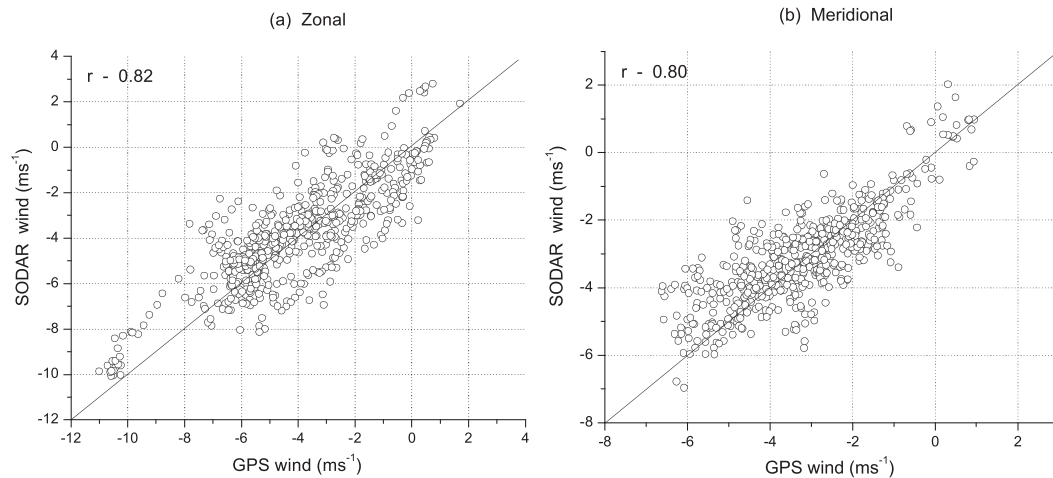
FIG. 6. Scatterplots of sodar wind velocity vs GPS sonde wind velocity for (a) zonal and (b) meridional components up to a height of 900 m in multifrequency output mode.

height of 600 m, whereas in the case of multifrequency transmission mode, it is up to 900 m. This demonstrates the advantage of using multifrequency transmission and reception for obtaining higher altitude coverage.

We have calculated another statistical parameter that is a standard deviation (σ_D) for better understanding of the results obtained. Here, standard deviation is calculated for overall observations by taking the difference of mean values of GPS sonde and sodar wind velocities. The statistics has been independently carried out for single-frequency and multifrequency transmission. For a single-frequency transmission, the standard deviation values are 1.54 m s^{-1} for zonal velocity and 1.63 m s^{-1} for meridional velocity. These are the averaged values over a height of 600 m; whereas in multifrequency output, the range is considered up to 900 m and the corresponding standard deviation values for zonal and meridional velocities are 1.34 and 1.35 m s^{-1}, respectively. More details of this statistics in different height

segments are presented in Table 3. We have also compared the single-frequency and multifrequency transmission. For this study data is considered up to the range of 600 m. Figure 7 shows the scatterplot between single-frequency and multifrequency transmission. A good correlation with a correlation coefficient of 0.91 for zonal winds and 0.90 for meridional winds is observed. This shows the self-consistency in the data produced with different frequencies and also the advantage of multifrequency transmission to get better altitude coverage.

5. Conclusions

Multifrequency decoding of phased array Doppler sodar has been successfully implemented. It is observed that multifrequency transmission has improved altitude coverage by 30% in wind profiling when compared to

TABLE 2. Correlation coefficients of zonal and meridional velocities for (a) GPS vs single frequency output and (b) GPS vs multifrequency output.

| (a) Height (m) | Correlation coefficient | |
	Zonal	Meridional
30–300	0.79	0.77
300–600	0.77	0.75
30–600	0.78	0.77
(b) Height (m)	Correlation coefficient	
	Zonal	Meridional
30–300	0.81	0.80
300–600	0.84	0.79
30–600	0.82	0.77
30–900	0.82	0.80

TABLE 3. Standard deviation of zonal and meridional velocities for (a) GPS vs single-frequency output and (b) GPS vs multifrequency output.

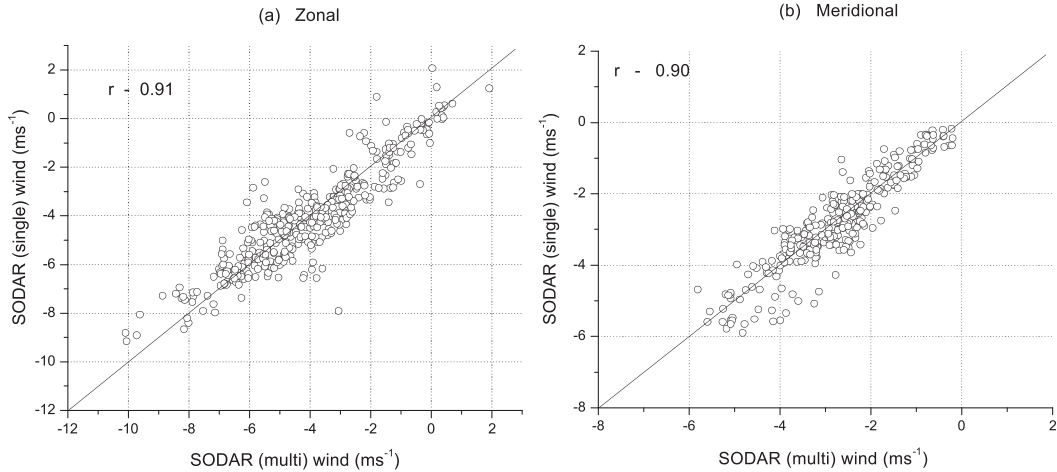| (a) Height (m) | Standard deviation (m s^{-1}) | |
	Zonal	Meridional
30–300	1.42	1.57
300–600	1.51	1.70
30–600	1.54	1.63
30–900	2.44	2.50
(b) Height (m)	Standard deviation (m s^{-1})	
	Zonal	Meridional
30–300	1.21	1.29
300–600	1.30	1.36
30–600	1.46	1.48
30–900	1.34	1.35

FIG. 7. Scatterplot wind velocity measured by sodar single-frequency output vs multifrequency output for (a) zonal and (b) meridional components up to a height of 600 m.

single-frequency transmission. The results are compared with GPS sonde measured winds. A very good comparison is obtained up to 600 m for single-frequency transmission and up to 900 m for multifrequency transmission and reception. Correlation analysis between GPS sonde and sodar measurement shows very good agreement in the observation window. Self-consistency between single-frequency and multifrequency is also carried out and shows excellent correlation. This demonstrates the advantage of using multifrequency transmission and reception for obtaining higher altitude coverage in wind profiling using sodar system.

APPENDIX A

Noise Level Estimation

There are many methods adapted to find out the noise level estimation. Basically all methods are statistical approximation to the near values. The method implemented here,

$$\frac{\text{Variance}(S)}{\text{mean}(S)} \leq 1 \text{ over number of spectra averaged,}$$

is based on the variance decided by a threshold criterion (Hildebrand et al. 1974). The noise level threshold shall be estimated to the maximum level L, such that the set of spectral points below the level S, nearly satisfies the criterion,

a. Step 1

Reorder the spectrum $\{P_i, \ i = 0, \ldots, N-1\}$ in ascending order to form. Let this sequence be written as $\{A_i, i = 0, \ldots, N-1\}$ and $A_i < A_j$ for $i < j$.

b. Step 2

Compute

$$P_n = \sum_{i=0}^{n} \frac{A_i}{(n+i)},$$

$$Q_n = \sum_{i=0}^{n} \frac{A_i^2}{(n+1)} - P_n^2,$$

and if $\quad Q_n > 0, \quad R_n = \frac{P_n^2}{Q_n M}, \quad$ for $\quad n = 1, \ldots, N,$

where M is the number of spectra that were averaged for obtaining the data.

c. Step 3

$$\text{Noise level } (L) = P_k$$

where

$$k = \min \begin{vmatrix} n \text{ such that } R_n > 1 \\ 1 \text{ if no } n \text{ meets the above criterion} \end{vmatrix}.$$

APPENDIX B

Moments Estimation

The extraction of the zeroth, first, and second moments is the key problem on doing all the signal processing and thereby finding out the various atmospheric and turbulence parameters in the region of radar sounding. The basic steps involved in the estimation of moments are given below.

a. Step 1

Reorder the spectrum to its correct index of frequency (i.e., $-f_{\text{maximum}}$ to $+f_{\text{maximum}}$) in the following manner:

Spectral	0	1	$N/2$	$N-1$
index	ambiguous f	$-f_{\text{maximum}}$	$f = 0$	$+f_{\text{maximum}}$

b. Step 2

Subtract noise level L from spectrum.

c. Step 3

1) Find the index of the peak value in the spectrum,

$$\tilde{P}_1 \geq \tilde{P}_i \quad \text{for all} \quad i = 0, \ldots, N-1.$$

2) Find m, the lower Doppler point of index from the peak point,

$$\tilde{P}_i \geq 0 \quad \text{for all} \quad m \leq i \leq l.$$

3) Find n the upper Doppler point of index from the peak point,

$$\tilde{P}_i \geq 0 \quad \text{for all} \quad l \leq i \leq n.$$

d. Step 4

The moments computed as

1) $M_0 = \sum_{i=m}^{n} \tilde{P}_i$

represents the zeroth moment or total power in the Doppler spectrum;

2) $M_1 = \dfrac{1}{M_0} \sum_{i=m}^{n} \tilde{P}_i f_i \quad \text{where} \quad f_i = \dfrac{[i - (N/2)]}{(\text{IPP} \times n \times N)}$

represents the first moment or mean Doppler in Hz [interpulse period (IPP)];

3) $M_2 = \dfrac{1}{M_0} \sum_{i=m}^{n} \tilde{P}_i (f_i - M_1)^2$

represents the second moment or variance, a measure of dispersion from central frequency.

REFERENCES

Anandan, V. K., P. Balamuralidhar, P. B. Rao, A. R. Jain, and C. J. Pan, 2005: An adaptive moments estimation technique applied to MST radar echoes. *J. Atmos. Oceanic Technol.,* **22,** 396–408.

——, M. Shravan Kumar, and I. Srinivasa Rao, 2008: First results of experimental tests of newly developed NARL phased array Doppler sodar. *J. Atmos. Oceanic Technol.,* **25,** 1778–1784.

Beran, D. W., C. G. Little, and B. C. Willmarth, 1971: Acoustic Doppler measurements of vertical velocities in the atmosphere. *Nature,* **230,** 160–162.

Brown, E. H., and F. F. Hall Jr., 1978: Advances in atmospheric acoustics. *Rev. Geophys. Space Phys.,* **16,** 47–110.

Clifford, S. F., J. C. Kaimal, R. J. Lataitis, and R. G. Strauch, 1994: Ground based remote profiling in atmospheric studies: An overview. *Proc. IEEE,* **82,** 313–355.

Coulter, R. L., and M. A. Kallistratova, 2004: Two decade progress in SODAR techniques. *Meteor. Atmos. Phys.,* **85,** 3–19.

Engelbart, D. A. M., M. A. Kallistratova, and R. D. Kouznetsov, 2007: Determination of turbulent fluxes of heat and momentum in the ABL by ground based remote-sensing techniques (a review). *Meteor. Z.,* **16,** 325–335.

Farley, D. T., 1985: On-line data processing techniques for MST radars. *Radio Sci.,* **20,** 1177–1184.

Giannini, L., S. Argentini, G. Mastrantonio, and L. Rossini, 1996: Estimation of flux parameters from sodar wind profiles. *Atmos. Environ.,* **31,** 1307–1313.

Hildeband, P. H., and R. S. Sekhon, 1974: Objective determination of the noise level in Doppler spectra. *J. Appl. Meteor.,* **13,** 808–811.

Kallistratova, M. A., and R. L. Coulter, 2004: Application of sodars in the study and monitoring of the environment. *Meteor. Atmos. Phys.,* **85,** 21–37.

Kouznetsov, R. D., 2008: Multi-frequency acoustic sounding of the ABL with a dish antenna. *IOP Conf. Ser. Earth Environ. Sci.,* **1,** 012038, doi:10.1088/1755-1315/1/1/012038.

——, V. F. Kramar, F. Beyrich, and D. Engelbart, 2004: Sodar-based estimation of TKE and momentum flux profiles in the atmospheric boundary layer: Test of a parameterization model. *Meteor. Atmos. Phys.,* **85,** 93–99.

——, ——, and M. A. Kallistratova, 2007: The vertical structure of turbulent momentum flux in the lower part of the atmospheric boundary layer. *Meteor. Z.,* **16,** 367–373.

Kramar, V. F., and R. D. Kouznetsov, 2002: A new concept for estimation of turbulent parameter profiles in the ABL using sodar data. *J. Atmos. Oceanic Technol.,* **19,** 1216–1224.

Mastrantonio, G., and G. Fiocco, 1982: Accuracy of wind velocity determinations with Doppler sodars. *J. Appl. Meteor.,* **21,** 823–830.

McAllister, L. G., 1968: Acoustic sounding of the lower troposphere. *J. Atmos. Terr. Phys.,* **30,** 1439–1440.

Neff, W. D., and R. L. Coulter, 1986: Acoustic remote sensing. *Probing the Atmospheric Boundary Layer*, D. H. Lenschow, Ed., Amer. Meteor. Soc., 201–239.

Woodman, R. F., 1985: Spectral moments estimation in MST radars. *Radio Sci.,* **20,** 1185–1195.